*inorganics*

MDPI

*Article*

# Thermal Shock Resistance of Commercial Oxide-Bonded Silicon Carbide Reticulated Foams under Concentrated Solar Radiation at PSA: A Feasibility Study

**Fernando de Almeida Costa Oliveira [1,*], José Galindo [2], José Rodríguez [2], Inmaculada Cañadas [2] and Jorge Cruz Fernandes [3]**

[1] LNEG—Laboratório Nacional de Energia e Geologia I.P., LEN—Laboratório de Energia, UME—Unidade de Materiais para a Energia, Estrada do Paço do Lumiar, 22, 1649-038 Lisboa, Portugal
[2] PSA—Plataforma Solar de Almería, CIEMAT—Centro de Investigaciones Energéticas, Medioambientales y Tecnológicas, Apartado 22, E-04200 Tabernas, Spain; jose.galindo@psa.es (J.G.); jose.rodriguez@psa.es (J.R.); inmaculada.canadas@psa.es (I.C.)
[3] IDMEC—Instituto de Engenharia Mecânica, Instituto Superior Técnico, Universidade de Lisboa, Av. Rovisco Pais, 1049-001 Lisboa, Portugal; cruz.fernandes@tecnico.ulisboa.pt
* Correspondence: fernando.oliveira@lneg.pt

**Abstract:** Volumetric ceramic receivers can be regarded as a promising technology to heat air above 1000 °C for solar thermal electricity production. In this study, the thermal shock behavior of commercial 10 ppi (A) and 20 ppi (B) oxide-bonded silicon carbide (ob-SiC) reticulated porous ceramic (RPC) foams was evaluated using the SF60 solar furnace at Plataforma Solar de Almería. The foams were subjected to well-controlled temperature cycles ranging from 800 to 1000, 1200, 1300 or 1400 °C, for 25, 100, and 150 cycles. The extent of the damage after thermal shock was determined by crushing tests. The damage was found to be critically dependent on both the bulk density and cell size. Decreasing both the bulk density and cell size resulted in better thermal shock resistance. The B foam exhibited approximately half the stress degradation compared to the A foam when exposed to a temperature difference of 600 K (in the range of 800 to 1400 °C) and subjected to 150 cycles.

**Keywords:** silicon carbide foams; solar furnace; concentrated solar radiation; thermal shock; crushing strength; open volumetric receivers



**Citation:** Costa Oliveira, F.d.A.; Galindo, J.; Rodríguez, J.; Cañadas, I.; Cruz Fernandes, J. Thermal Shock Resistance of Commercial Oxide-Bonded Silicon Carbide Reticulated Foams under Concentrated Solar Radiation at PSA: A Feasibility Study. *Inorganics* **2024**, *12*, 246. https://doi.org/10.3390/inorganics12090246

Academic Editor: Roberto Nisticò

Received: 24 July 2024
Revised: 27 August 2024
Accepted: 4 September 2024
Published: 11 September 2024



## 1. Introduction

The usage of solar energy is one way to increase the sustainability of production processes using a renewable and carbon free heating source [1–3]. Among the solar approaches available, concentrated solar power (CSP) tower technology is well established [4]. It relies on concentrating light through mirrors onto a receiver (also called an absorber) [5,6]. Many studies were conducted on suitable materials for solar receivers, including SiC fiber mesh Ceramat® FN, supplied by Schott Glass (Mainz, Germany), SiC monoliths manufactured by HelioTech (Svenstrup, Denmark), and SiC foams [7,8]. Wang et al. [9] performed thermal analysis of the porous media receiver by combining the Monte Carlo Ray Tracing method with FLUENT software but did not mention the morphology of the SiC foam tested on a solar dish collector. A similar approach has been employed by Kribus et al. [10] for an open receiver made of SiC foam, suggesting that the available commercial materials offered a limited range of features that are still not optimal for the application. Optimization of geometry (porosity and pore size) appears to be insufficient to reach a high efficiency, whilst a double layer SiC foam holds great potential to enhance efficiency. This is attributed to the fact that the thickness of the first porous layer has a significant effect on the temperature distribution and pressure drop.

On the other hand, Lidor et al. [11] showed that there is a significant temperature gradient across large scale porous absorbers. Development of new thick, porous materials

for volumetric air receivers is therefore important. In this respect, one must bear in mind that the extinction coefficient is another key parameter for estimating radiation properties in porous media, as it enables the determination of the radiative thermal conductivity [12]. It has been shown that the extinction coefficient increases with both decreasing porosity and pore size [13]. Furthermore, high optical thicknesses (larger pore sizes) favor more homogenous temperature gradients across thicker ceramic foams, as the concentrated solar beam can penetrate deep inside the porous structure [14].

A 5-kW solar receiver prototype proved to deliver a high-temperature air flow (>1000 °C) with a reasonably high thermal efficiency (>0.65) using 10 ppi (pores per inch) SiSiC foams [15]. Thence, there is plenty of room for improvement on both the geometry and the material properties for large scale absorbers. Indeed, challenges associated with durability, receiver efficiency, and the specific cost remain to be sorted out. The inherent advantages of air receivers, such as availability of the fluid, no trace heating necessary, non-toxic, and 3–5 h of thermal storage, allow higher-efficiency thermodynamic cycles, and the high receiver thermal efficiency (>75% due to the volumetric effect which reduces thermal radiation losses) makes this technology simpler, cheaper, and more efficient than other currently available technologies [16]. However, the material's suitability and its durability still need to be addressed in a suitable fashion. Among the current solar receivers, three major types exist, namely: (a) Surface receivers (tubular, external, cavity), (b) Porous receivers (wire mesh, ceramic/metallic foams, honeycombs), and (c) Particle receivers (falling curtain, entrained particles), according to Mey-Coltier et al. [17]. Exploiting the 3D structure and properties of ceramic foams in this kind of application can open new routes for producing heat from solar irradiation. First used in liquid metal filtration, reticulated porous ceramic (RPC) foams are currently being used as gas (particulate) filters, kiln furniture, catalyst substrates, porous burner substrates, scaffolds for bone regeneration, advanced thermal management, heat exchangers, and bacteria/cell immobilization, among others [18,19].

The present study aimed at evaluating the damage imposed on two commercial oxide-bonded silicon carbide reticulated porous ceramic foams, hereafter referred to as ob-SiC RPC foams, having pore densities of 10 and 20 ppi (pores per inch), through exposure to concentrated solar radiation, under drastic thermal shock conditions, replicating those experienced by real solar open volumetric air receivers. The development of solar thermal energy conversion processes faces challenges related to receiver/reactor materials and radiative energy distribution technology. Recently, innovative approaches to efficient solar energy conversion have been developed using complex coupled numerical models applied to a high-flux solar reactor and a simulator [20]. Before widespread use, the suitability and cyclic stability of the materials must be demonstrated. To the best of the author's knowledge, such data has not yet been reported in the open literature for commercial ob-SiC RPC foams, which would be useful for modelling purposes.

The simplest way to assess thermal shock resistance is by rapidly transferring the heated samples from a resistance furnace to a quenching bath containing distilled water at room temperature. Thus, for comparison purposes, the ob-SiC RPC foams under investigation were kept at a soaking temperature (namely 420 and 620 °C) for 1 h prior to quenching. The damage was assessed by measuring the retained crushing strength after water quenching tests at various temperature differences, $\Delta T$, which are defined as the pre-set temperature of the samples minus the temperature of the bath, typically at 20 °C. The resistance to thermal shock of the dense ceramics is found to fall in an abrupt fashion, whereas in the case of RPC foams it was found that the crushing strength retained undergoes a gradual decrease with increasing quench temperature because of an increase in mechanical damage throughout the material. A similar trend was observed for thermal shock tests carried out on cordierite foams [21].

Regarding the current state of the art, thermal shock was assessed by means of an innovative experimental setup, developed at PSA, including a guillotine system, a secondary concentrator, and a temperature control system, which allowed the performance of

thermal shock cycles under conditions that cannot be realized in conventional electrical or gas furnaces [22].

Thermal cycling of the ob-SiC RPC foams under direct solar irradiation is regarded as an interesting alternative to the current honeycombs based on siliconized silicon carbide commonly used in pilot power plants, not only in terms of cost, but also performance [23–25]. After cycling, the retained crushing strength was measured, and the results are quite promising.

## 2. Results

### *2.1. Materials Characterization*

Table 1 summarizes the bulk densities ($\rho_b$) and porosities of the tested materials under investigation. The true density of the ob-SiC RPC strut material ($\rho_r$) was determined by He pycnometry to be 3.01 ± 0.01 Mg m$^{-3}$. Therefore, the maximum porosity was of about 87%, bearing in mind that $P = 1 - (\rho_b/\rho_r) = 1 - (0.38/3.01)$.

**Table 1.** Samples characteristics.

| Pore Size (ppi) | Bulk Density [1] (Mg m$^{-3}$) | Relative Density | Porosity (%) |
|---|---|---|---|
| 10 | 0.46 ± 0.01 | 0.15 | 85 |
| 20 | 0.38 ± 0.01 | 0.13 | 87 |

[1] mean ± SD of 10 samples.

The macrostructure of the as-received foams is shown in Figure 1. Typically, the mean thickness of the struts ranged from 0.75 ± 0.20 mm and 0.45 ± 0.15 mm, for the 10 ppi and 20 ppi foams, respectively. The linear intercept method was used to determine the cell size and the values obtained match the specification.

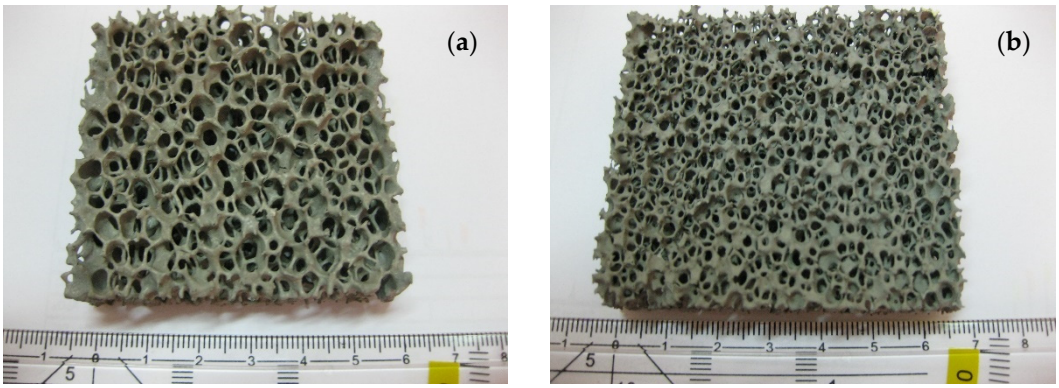


**Figure 1.** Top view of as-received 10 ppi (**a**) and 20 ppi (**b**) ob-SiC RPC foams.

The X-ray diffraction (XRD) profiles of the as-received and exposed ob-SiC RPC foams, after grinding into powder form using an agate mortar, are shown in Figure 2. The diffraction patterns, in the range of 20° < 2θ < 75°, show peaks corresponding to the planes, which match with the pattern of the ICDD data base, having the card no. 01-072-0018 (corresponding to the phase Moissanite-6H-SiC/●/) and traces of Moissanite-4H-SiC/□/(ICDD card no. 029-1127), $SiO_2$/◊/(ICDD card no. 039-1425) and $Al_2O_3$/○/(ICDD card no. 01-070-7346).

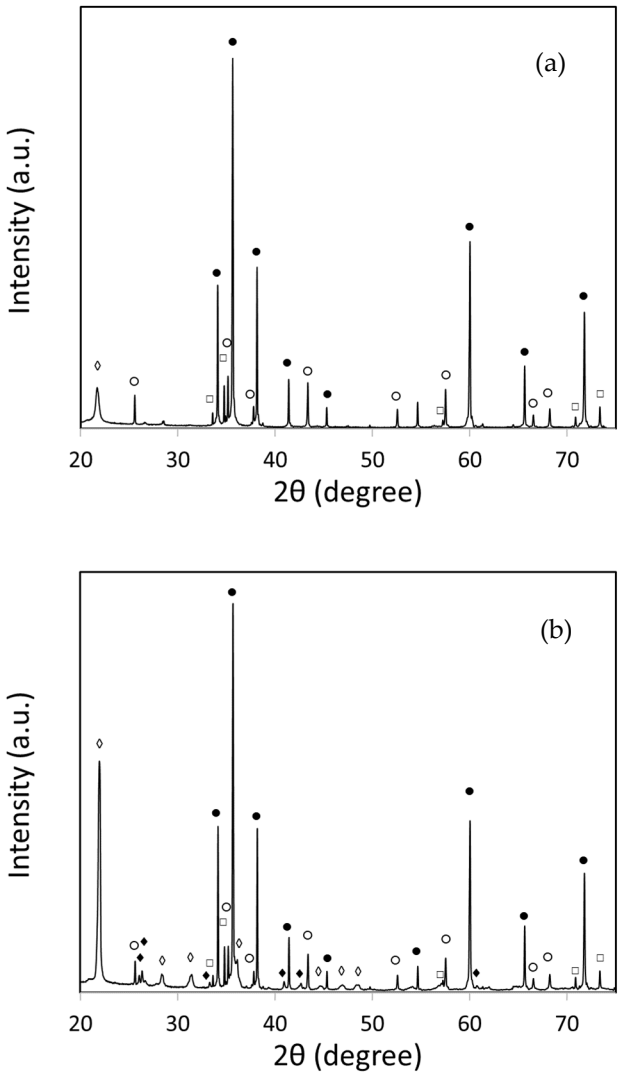


**Figure 2.** Typical XRD patterns of ob-SiC RPC foam before (**a**) and after exposure at 1400 °C for 150 cycles (**b**).

After exposure to 1400 °C for 150 cycles, oxidation of the ob-SiC RPC foams took place as indicated by the increase in the intensity of the peaks matching the $SiO_2$ phase and the formation of minor amounts of mullite ($Al_6Si_2O_{13}$)/♦/(ICDD card no. 015-0776).

### *2.2. Thermal Shock*

To evaluate the damage imposed on reticulated porous ceramic (RPC) materials, namely commercial silicon carbide foams having pore densities of 10 and 20 ppi, thermal shock cycling was performed under conditions replicating those experienced by real solar open volumetric air receivers through direct exposure to concentrated solar radiation.

Most thermal performance data available refer to tests performed using xenon lamps simulators, so information regarding the effect of the entire wavelengths spectrum of solar radiation reaching the materials surface on their degradation is not known with certainty. Five new porous morphologies suitable for volumetric solar receivers have been analyzed experimentally in a laboratory-scale solar simulator in terms of the efficiency of the absorber's thermal performance, but no data have been provided on their mechanical performance [26]. It is therefore pertinent to address this issue, particularly resistance to thermal shock. In this study, ten thermal shock tests were undertaken in the SF60 solar furnace of PSA under well-controlled conditions listed in Table 4.

Figure 3 shows the temperature distribution over the top surface exposed area of the foams. The maximum deviation observed between the target value (point 1) and the temperature measured at the middle of each of the four exposed samples was around 30 °C. The temperature measured by the IR camera was similar to that measured by the B1 thermocouple.

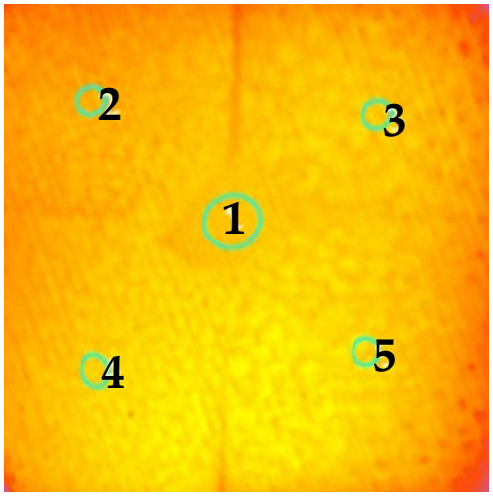


| Point | T (°C) |
|---|---|
| 1 | 1402 ± 13 |
| 2 | 1376 ± 20 |
| 3 | 1426 ± 17 |
| 4 | 1421 ± 18 |
| 5 | 1430 ± 17 |

**Figure 3.** Temperature distribution over the exposed top surface area showing typical temperatures measured using the IR camera when the maximum temperature was set at 1400 °C.

The temperature measured by the thermocouple B1 was therefore used to control the shutter opening/closing for performing the thermal cycles shown in Figure 4.

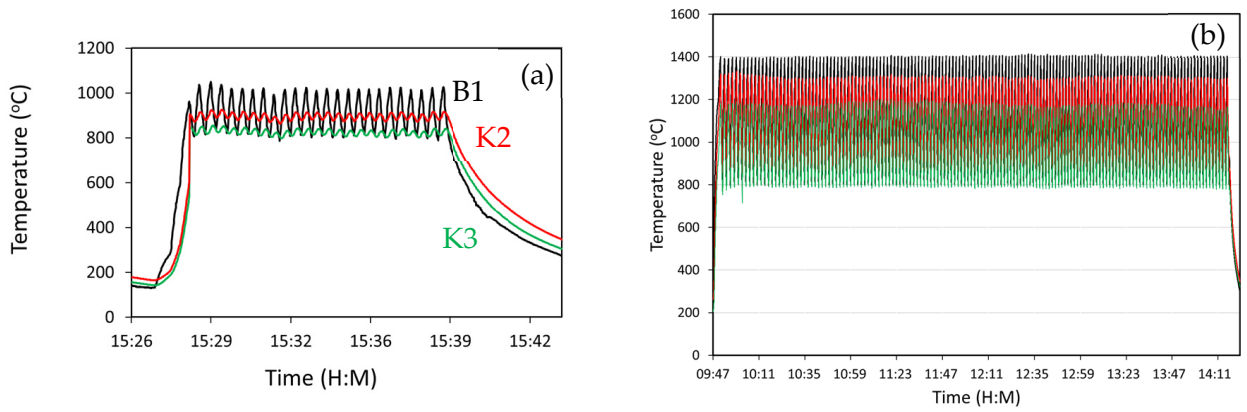


**Figure 4.** Temperature versus time graphs at ΔT = 600 K after 25 cycles (**a**) and 150 cycles (**b**) for 10 ppi ob-SiC RPC foam showing profiles measured by thermocouples B1 (black), K2 (red) and K3 (green).

### *2.3. Oxidation Data*

Table 2 lists the mass changes recorded before and after the thermal shock tests. Oxidation is more evident on the top surface than on the bottom one, as denoted by the darker surface appearance (Figure 6d), particularly at temperature above 1200 °C. At ΔT = 200 K, no mass change was observed after 25 cycles.

**Table 2.** Mass changes (in %) of the exposed 10 ppi (**A**) and 20 ppi (**B**) ob-SiC RPC foams.

| (A) | | | | |
|---|---|---|---|---|
| **N°. Cycles** | **ΔT (K)** | | | |
| | 200 | 400 | 500 | 600 |
| 25 | 0 | 0.04 ± 0.01 | 0.36 ± 0.17 | 1.77 ± 0.65 |
| 100 | | 0.28 ± 0.03 | 1.37 ± 0.32 | 2.68 ± 0.39 |
| 150 | | 0.99 ± 0.20 | 1.47 ± 0.06 | 3.30 ± 0.67 |
| (B) | | | | |
| **N°. Cycles** | **ΔT (K)** | | | |
| | 200 | 400 | 500 | 600 |
| 25 | 0 | 0.25 ± 0.03 | 0.61 ± 0.08 | 1.23 ± 0.49 |
| 100 | | 0.38 ± 0.03 | 1.69 ± 0.51 | 2.26 ± 0.08 |
| 150 | | 0.89 ± 0.05 | 1.72 ± 0.52 | 2.99 ± 0.81 |

### *2.4. Crushing Data*

Subjecting the top surface of the ob-SiC RPC foams to rapid change in temperature produces a thermal stress distribution, the magnitude of which depends on the heat transfer coefficient at the surface relative to the rate at which heat can be conducted to or from the surface through the bulk.

Representative curves of crushing strength versus strain are shown in Figure 5. It was observed that a macrocrack propagated through the compressed foam when the slope of the curve changed. For this reason, the value corresponding to such change was considered as the rupture stress.

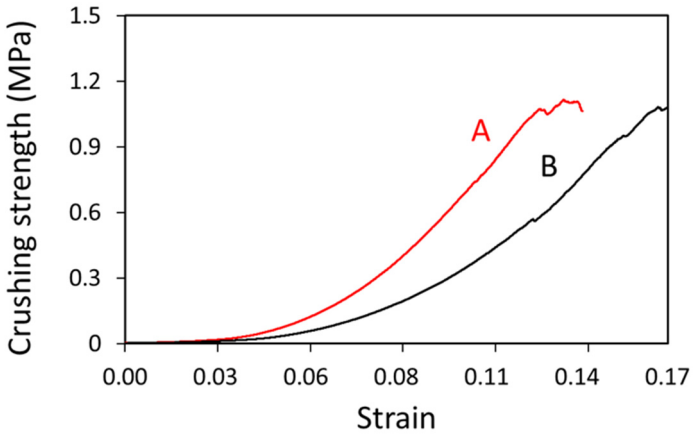


**Figure 5.** Typical crushing strength curves for foams A and B tested at ΔT = 600 K for 150 cycles.

The mean values of crushing strength are listed in Table 3 highlighting the effect of both oxidation and thermal stresses on their retained structural integrity.

**Table 3.** Crushing strength data obtained for the different testing conditions.

| **Foam** | | **Number of Cycles** | | | | |
|---|---|---|---|---|---|---|
| **A (10 ppi)** | **ΔT (K)** | **0** | **1** | **25** | **100** | **150** |
| | 200 | | | 0.70 ± 0.01 | | |
| | 400 | | | 0.59 ± 0.04 | 0.56 ± 0.02 | 0.58 ± 0.01 |
| | 500 | | | 0.60 ± 0.02 | 0.55 ± 0.01 | 0.52 ± 0.01 |
| | 600 | | | 0.57 ± 0.02 | 0.56 ± 0.02 | 0.53 ± 0.02 |
| | As-received | 0.70 ± 0.01 | | | | |
| | 400 ($H_2O$) | | 0.52 ± 0.02 | | | |
| | 600 ($H_2O$) | | 0.50 ± 0.02 | | | |

**Table 3.** *Cont.*

| | | Number of Cycles | | | | |
|---|---|---|---|---|---|---|
| **B (20 ppi)** | **ΔT (K)** | **0** | **1** | **25** | **100** | **150** |
| | 200 | | | 0.67 ± 0.01 | | |
| | 400 | | | 0.65 ± 0.01 | 0.59 ± 0.07 | 0.60 ± 0.01 |
| | 500 | | | 0.64 ± 0.01 | 0.59 ± 0.04 | 0.60 ± 0.04 |
| | 600 | | | 0.61 ± 0.02 | 0.58 ± 0.01 | 0.59 ± 0.01 |
| | As-received | 0.67 ± 0.01 | | | | |
| | 400 ($H_2O$) | | 0.62 ± 0.01 | | | |
| | 600 ($H_2O$) | | 0.56 ± 0.02 | | | |

## 3. Discussion

The damage associated with oxidation was determined by the mass change upon exposure to the concentrated solar beam, owing to the oxidation of silicon carbide into silica, according to the reaction:

$$SiC\ (s) + 3/2\ O_2\ (g) \rightarrow SiO_2\ (s) + CO\ (g) \quad (1)$$

as confirmed by XRD analysis (Figure 2). This results in the formation of a surface $SiO_2$ (cristobalite) layer, which protects the substrate and alters the surface condition [27]. In addition, $SiO_2$ reacts with $Al_2O_3$ leading to the formation of mullite ($3Al_2O_3{\cdot}2SiO_2$) [28]. The mass change increased with increasing either ΔT or the number of cycles, as expected, mainly due to the oxidation of the SiC. In the same way as silicon nitride, it is expected that thermal cycling will have a minimal effect on the rate of oxidation. However, it could affect the characteristics of the oxidation products on the surface, depending on how often the cycling occurs. Whilst the oxide layers develop cracks upon cooling, they quickly heal when exposed to high temperatures again. There was no observable change in the mechanism controlling the rate of oxidation during the investigated exposure time [29].

Beside degradation caused by oxidation, the thermal stresses imposed on the foams upon thermal cycling are expected to damage the structural integrity of the materials.

The current setup permitted to accomplish a more or less homogenous temperature distribution (±30 °C) over the irradiated surface (Figure 3). However, when the control temperature (B1) varied from 800 to 1000 °C, the thermocouples placed underneath K2 and K3 (Figure 6e) fell in the range of 880 ± 5 °C to 920 ± 10 °C (difference of about 80 °C compared to B1) and 800 ± 5 °C to 850 ± 10 °C, respectively, as can be seen in Figure 4. The maximum temperature difference between the top and bottom surfaces' temperatures set and those actually measured was about 150 °C.

In the case of the temperature (B1) ranged from 800 to 1400 °C, the thermocouples K2 and K3 ranged from 870 ± 5 °C to 1300 ± 20 °C (difference of about 100 °C compared to B1) and 785 ± 5 °C to 1175 ± 15 °C (indicating that the difference from the top surface temperature was around 200 °C), respectively. This shows that the actual temperature gradients across each sample varied from 600 K (on the radiated surface) to about 400 K (non-radiated one). As expected, the samples were subjected to several temperature gradients, namely across their thickness and their width, resulting in unknown thermal stress fields.

The crushing strength of the RPC foams is known to depend on their relative porosity [30]. In the present case, the difference in porosity is small (85 and 87%), so its effect is low: the as-received crushing strength decreased from 0.70 ± 0.01 to 0.67 ± 0.01 MPa, going from 10 ppi to 20 ppi ob-SiC RPC foams, respectively. Using the bending micromechanical model developed by Gibson and Ashby [31], one can estimate the compressive strength of an open-cell ceramic foam, $\sigma_{cf}$, through the relationship:

$$\sigma_{cf} = C_1 \sigma_{fs} \left( \frac{\rho_{cf}}{\rho_s} \right)^{\frac{3}{2}} \quad (2)$$

where $\sigma_{fs}$ is the flexural strength of the strut material (assumed to be 40 MPa [32]), $\rho_{cf}$ is the bulk density of the ceramic foam, $\rho_s$ is the density of the solid struts (3.01 Mg $m^{-3}$, measured by pycnometry), and $C_1$ is a geometric constant characteristic of the unit cell shape. The value of $C_1$ was found to be equal to 0.16, by Zhang and Ashby, for brittle open-cell foams assuming tetrakaidecahedral unit cell geometry [33]. For the 10 ppi foam, the $\rho_{cf}$ = 0.46 Mg $m^{-3}$ and the calculated $\sigma_{cf}$ is 0.38 MPa (i.e., about 50% lower than that measured experimentally). This discrepancy is attributed to the fact that the tested foams contained four external solid walls (Figure 6d). For A foams (10 ppi), increasing the ΔT from 200 to 600 K resulted in a crushing strength decrease of 18.6% after 25 cycles and 24.3% after 150 cycles. In contrast, the decrease in crushing strength for B foams (20 ppi) was around 9% and ≈12% after 150 cycles under the same conditions (Table 3). At ΔT = 600 K, for A foams the decrease in strength was around 7% when increasing the number of cycles from 25 to 150. In the case of the B-type foams, under the same conditions, the decrease was roughly half (3.3%).

The thermal shock stresses imposed on the foams when testing them in water baths is more severe than that experienced upon solar exposure. For ΔT = 400 K, the retained crushing strength dropped ≈26% and ≈8% for type A and B foams, respectively. In the case of ΔT = 600 K, the decrease was respectively ≈29% and ≈16% for type A and B foams. One can therefore assume that ΔTc for the A foams is 600 K. The results obtained showed that the thermal shock resistance of the B foam is better than their A foam counterparts (both in air and water media). Experiments using ceramic foams showed that very high porosities (>70%) result in thermal shock resistance improvements, which is attributed to penetration of the foam structure by the cooling medium [34]. Indeed, such open-cell foams are characterized by a very high permeability, with larger cell sizes facilitating the infiltration of the structure by the quenching media. At least two sources of thermal stress can thus be considered: one associated with the heating of the quenching medium as it infiltrates the cellular structure; and the other the temperature gradient across the microscopic struts [35]. The former temperature gradient seems to be more pronounced than the latter one in the present work, as the thermal shock resistance was found to increase with decreasing in cell size, which was also observed for cordierite foams [21].

The experimental data obtained are in good agreement with those published for similar SiC foams, where foams having high ppi resulted in the best solar-to-thermal performances [17,36].

## 4. Materials and Methods

### *4.1. Materials*

The two commercial ob-SiC RPC foams manufactured by Vesuvius GmbH (Borken, Germany) were SEDEX 65 × 65 × 18 mm, 20 ppi (pores per inch) and SEDEX 60 × 60 × 18, 10 ppi, respectively. Their crystal structure was analyzed by XRD on a PANalytical's X'Pert PRO MPD diffractometer with a step size of 0.02° and the accelerating voltage of 40 kV. Phase identification was carried out with the DIFFRAC.EVA V7 software and the ICDD (International Centre for Diffraction Data). The measured density of the foams was determined using their mass and geometrical dimensions. The true density of the foams was measured by Helium pycnometry (Accupyc 1330, Micromeritics Inc., Norcross, GA, USA).

### *4.2. Thermal Cycling*

Experiments were carried out at the renewed SF60 solar furnace of PSA described by Rodríguez et al. [37] shown in Figure 6.

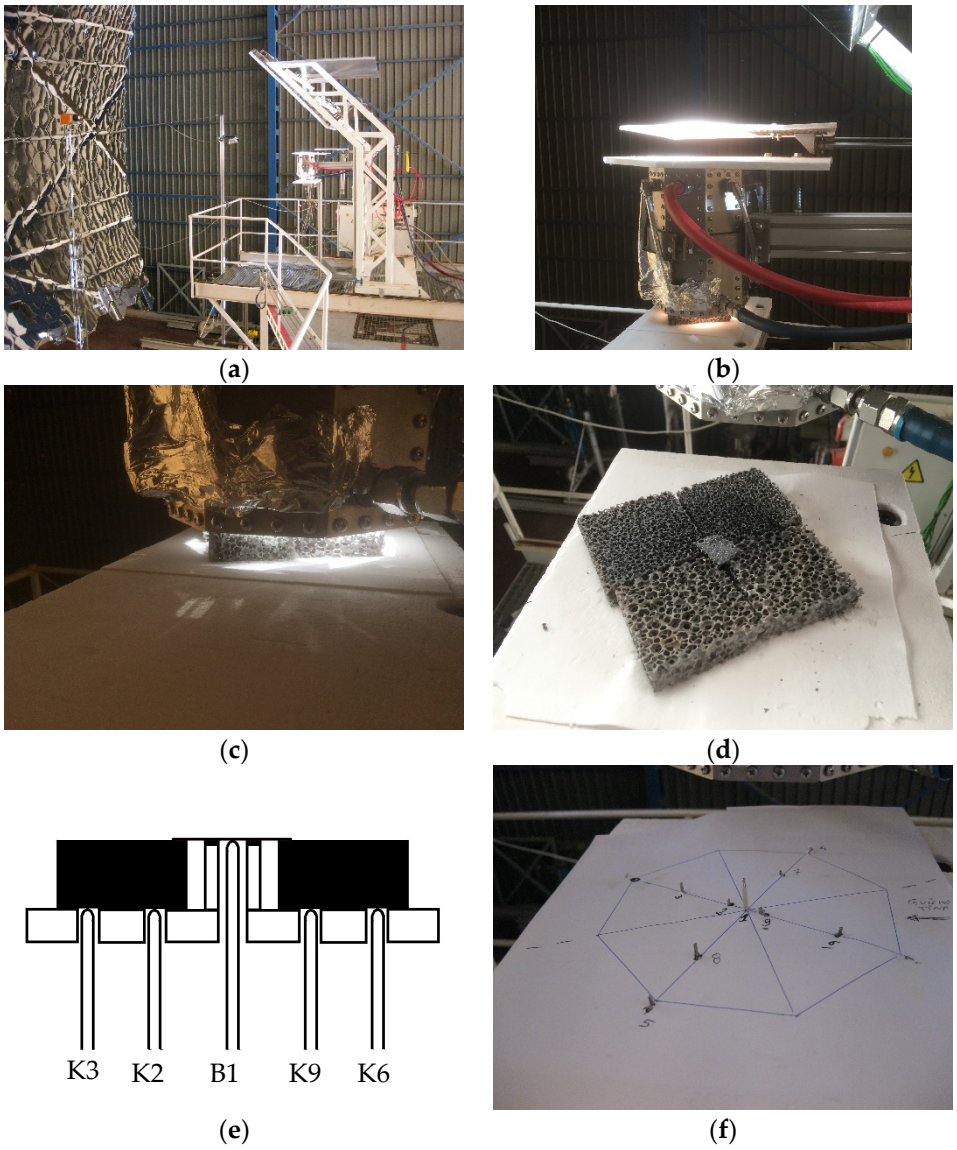


**Figure 6.** Experimental system showing the uncut (**a**) and in cut (**b**) guillotine positions; ob-SiC RPC samples being exposed (**c**); samples after the test at ΔT = 500 K for 100 cycles (**d**); scheme of the B- and K-type thermocouples positions (**e**); actual (nine) thermocouples positioning (**f**).

Briefly, this facility reaches a peak flux of 6722 kW $m^{-2}$ in a focus diameter of 22 cm. The optical axis of the furnace is horizontal, so that the HT130 heliostat, and the parabolic concentrator, allow the solar beam to be aligned on the optical axis of the parabola. The amount of incident sunlight was controlled through the angular motion of attenuator slats. Furthermore, a mirror placed at 45° was used to carry out the tests in the horizontal plane.

Owing to the Gaussian energy distribution of the concentrated solar beam, a secondary concentrator of octagonal shape, hereafter referred to as homogenizer, was placed in line to obtain a more homogeneous temperature distribution over the horizontal plane.

Ten thermal shock tests were carried out during the 10-working day campaign (from the 5th to the 16th of September 2022), according to the conditions listed in Table 4. In order to control the guillotine's on/off cycle, and consequently, the heating and cooling times, a specially designed LabView program was implemented. Cooling was achieved under natural conditions.

**Table 4.** Thermal cycling test conditions.

| ΔT (°C) | Heating Time (s) | Cooling Time (s) | Number of Cycles | | |
|---|---|---|---|---|---|
| | | | 25 | 100 | 150 |
| 800–1000 | 15 | 15 | x | - | - |
| 800–1200 | 35 | 45 | x | x | x |
| 800–1300 | 40 | 45 | x | x | x |
| 800–1400 | 45 | 50 | x | x | x |

For every test condition, two samples of each type of foam were exposed to the direct concentrated solar beam. The temperature recorded for the B-type thermocouple was used as the control reference for performing the thermal cycles. Underneath each exposed foam, two K-type thermocouples were placed as shown in Figure 6f. The measurements of the temperature distribution across the surface of the exposed foams were also carried out using an infra-red (IR) camera (model Equus 327k SM PRO), manufactured by IRCam GmbH, Erlangen, Germany. A flat piece of silicon carbide wall circa 1 mm thick was placed above the B-type thermocouple to measure the samples' surface temperature and compare it with both the solar-blind pyrometer (Infratherm IGA 5LO, IMPAC Electronic GmbH, Frankfurt, Germany) and the IR camera measurements (Figure 6d).

For comparison, water quenching tests were performed by rapid heat transfer of a test sample at an elevated temperature in a distilled water bath at room temperature according to the ASTM C1525-04 standard [38]. Two temperature differences were set: 400 and 600 K. The thermal shock resistance is defined as a critical temperature interval (ΔTc), which corresponds to at least 30% reduction in the mean retained strength.

To assess oxidation damage, prior and after each test the samples were weighed for mass change measurements.

### *4.3. Crushing Testing*

After cycling, the retained crushing strength was determined at room temperature using an Instron Corp., Norwood, MA, USA (model 4302) testing machine with the compressive plates closing at a crosshead speed of 0.5 mm min-1 with a load cell of 10 kN. Since the foams have four external walls, the procedure used to calculate the "crushing strength" was the same as described elsewhere [39]. Briefly, a compliant 1 mm thick rubber spacer was inserted between the loading plates and the foams to ensure uniform loading. On the other hand, the nominal load value required to calculate the "crushing strength" was determined as the point in the chart curve were the slope changed.

## 5. Conclusions

The purpose of the present study was to evaluate the ability of commercial ob-SiC RPC foams as solar receivers for new CSP plants. For this purpose, a dedicated experimental setup was developed allowing a ±30 °C temperature distribution over the entire irradiated surface plane to be achieved. The following conclusions could be drawn:

- The ob-SiC RPC foams showed good performance to thermal shock under the conditions investigated;
- The B foam having both lower bulk density and cell size showed better thermal shock behavior;
- Under the most extreme conditions (ΔT = 600 K, 150 cycles), the B foam (20 ppi) showed a crushing strength degradation of nearly half of the A foam (10 ppi) counterparts;
- Exposure of the foams to the thermal cycling resulted in the formation of a $SiO_2$-rich surface layer containing traces of mullite;
- The cooling medium effect on the retained crushing strength was found to be ΔTc = 600 K for A foam;

- The experimental crushing strengths were found to be about double of the predicted by the Gibson-Ashby model, which can be attributed to the fact that outer solid walls are present.
- Future work should focus on evaluating long-term durability, conducting a higher number of thermal cycles, and introducing an air stream during cooling to simulate real appliance conditions.

**Author Contributions:** Conceptualization, F.d.A.C.O. and J.C.F.; methodology, J.G., J.R. and I.C.; software, J.R.; validation, F.d.A.C.O. and J.C.F.; formal analysis, F.d.A.C.O. and J.C.F.; investigation, F.d.A.C.O., I.C. and J.C.F.; resources, J.C.F.; data curation, F.d.A.C.O. and J.C.F.; writing—original draft preparation, F.d.A.C.O. and J.C.F.; writing—review and editing, F.d.A.C.O., J.G., J.R., I.C. and J.C.F.; visualization, F.d.A.C.O. and J.C.F.; supervision, F.d.A.C.O. and J.C.F.; project administration, F.d.A.C.O.; funding acquisition, F.d.A.C.O. and J.C.F. All authors have read and agreed to the published version of the manuscript.

**Funding:** The funding provided by the European Commission through the SFERA-III project (Grant Agreement No. 823802) is acknowledged. The study was also financially supported by Fundação para a Ciência e a Tecnologia (FCT) via the project LAETA Base Funding (DOI: 10.54499/UIDB/50022/2020), and the INIESC-National Research Infrastructure for Concentrated Solar Energy through contract ALT20-03-0145-FEDER-022113.

**Data Availability Statement:** The datasets generated during and/or analyzed during the current study are available from the corresponding author upon reasonable request.

**Acknowledgments:** F.d.A.C.O. and J.C.F. gratefully acknowledge the CIEMAT-PSA Laboratory for providing access to its installations. The administrative support of Marta Ruiz is also appreciated. SEDEX filters were kindly donated by Foseco Portugal—Produtos para Fundição, Lda., Porto, Portugal.

**Conflicts of Interest:** The authors declare no conflicts of interest.

## References

1. Farjana, S.H.; Huda, N.; Parvez Mahmud, M.A.; Saidur, R. Solar process heat in industrial systems—A global review. *Renew. Sust. Energy Rev.* **2018**, *82 Pt 3*, 2270–2286. [CrossRef]
2. Ravi Kumar, K.; Krishna Chaitanya, N.V.V.; Sendhil Kumar, N. Solar thermal energy technologies and its applications for process heating and power generation—A review. *J. Clean. Prod.* **2021**, *282*, 125296. [CrossRef]
3. Kumar, L.; Ahmed, J.; El Haj Assad, M.; Hasanuzzaman, M. Prospects and challenges of solar thermal for process heating: A comprehensive review. *Energies* **2022**, *15*, 8501. [CrossRef]
4. Aprà, F.M.; Smit, S.; Sterling, R.; Loureiro, T. Overview of the enablers and barriers for a wider deployment of CSP tower technology in Europe. *Clean Technol.* **2021**, *3*, 377–394. [CrossRef]
5. Ávila-Marín, A.L. Volumetric receivers in solar thermal power plants with central receiver system technology: A review. *Sol. Energy* **2011**, *85*, 891–910. [CrossRef]
6. Ho, C.K. Advances in central receivers for concentrating solar applications. *Sol. Energy* **2017**, *152*, 38–56. [CrossRef]
7. Fend, T.; Hoffschmidt, B.; Pitz-Paal, R.; Reutter, O.; Rietbrock, P. Porous materials as open volumetric solar receivers: Experimental determination of thermophysical and heat transfer properties. *Energy* **2004**, *29*, 823–833. [CrossRef]
8. Roldán, M.I.; Smimova, O.; Fend, T.; Casas, J.; Zarza, E. Thermal analysis and design of a volumetric solar absorber depending on the porosity. *Renew. Energy* **2014**, *62*, 116–128. [CrossRef]
9. Wang, F.; Shuai, Y.; Tan, H.; Yu, C. Thermal performance analysis of porous media receiver with concentrated solar irradiation. *Int. J. Heat Mass Transf.* **2013**, *62*, 247–254. [CrossRef]
10. Kribus, A.; Gray, Y.; Grijnevich, M.; Mittelman, G.; Mey-Cloutier, S.; Caliot, C. The promise and challenge of solar volumetric absorbers. *Sol. Energy* **2014**, *110*, 463–481. [CrossRef]
11. Lidor, A.; Fend, T.; Roeb, M.; Sattler, C. Parametric investigation of a volumetric solar receiver-reactor. *Sol. Energy* **2020**, *204*, 256–269. [CrossRef]
12. Hajimirza, S.; Sharadga, H. Learning thermal radiative properties of porous media from engineered geometric features. *Int. J. Heat Mass Transf.* **2021**, *179*, 121668. [CrossRef]
13. Zhao, Y.; Tang, G.H. Monte Carlo study on extinction coefficient of silicon carbide porous media used for solar receiver. *Int. J. Heat Mass Transf.* **2016**, *92*, 1061–1065. [CrossRef]
14. Nimvari, M.E.; Jouybari, N.F.; Esmaili, Q. A new approach to mitigate intense temperature gradients in ceramic foam solar receivers. *Renew. Energy* **2018**, *122*, 206–215. [CrossRef]

15. Patil, V.R.; Kiener, F.; Grylka, A.; Steinfeld, A. Experimental testing of a solar air cavity-receiver with reticulated porous ceramic absorbers for thermal processing at above 1000 °C. *Sol. Energy* **2021**, *214*, 72–85. [CrossRef]
16. Ávila-Marín, A.L.; Caliot, C.; Flamant, G.; Alvarez de Lara, M.; Fernandez-Reche, J. Numerical determination of the heat transfer coefficient for volumetric air receivers with wire meshes. *Sol. Energy* **2018**, *162*, 317–329. [CrossRef]
17. Mey-Cloutier, S.; Caliot, C.; Kribus, A.; Gray, Y.; Flamant, G. Experimental study of ceramic foams used as high temperature volumetric solar absorber. *Sol. Energy* **2016**, *136*, 226–235. [CrossRef]
18. Fey, T.; Betke, U.; Rannabauer, S.; Scheffler, M. Reticulated replica ceramic foams: Processing, functionalization, and characterization. *Adv. Eng. Mater.* **2017**, *19*, 1700369. [CrossRef]
19. Hammel, E.C.; Ighodaro, O.L.-R.; Okoli, O.I. Processing and properties of advanced porous ceramics: An application based review. *Ceram. Int.* **2014**, *40*, 15351–15370. [CrossRef]
20. Lougou, B.G.; Wu, L.; Ma, D.; Geng, B.; Jiang, B.; Han, D.; Zhang, H.; Łapka, P.; Shuai, Y. Efficient conversion of solar energy through a macroporous ceramic receiver coupling heat transfer and thermochemical reactions. *Energy* **2023**, *271*, 126989. [CrossRef]
21. Costa Oliveira, F.A.; Dias, S.; Fernandes, J.C. Thermal shock behaviour of open-cell cordierite foams. *Mater. Sci. Forum* **2006**, *514–516*, 764–767. [CrossRef]
22. Costa Oliveira, F.A.; Fernandes, J.C.; Galindo, J.; Rodríguez, J.; Canãdas, I.; Rosa, L.G. Thermal resistance of solar volumetric absorbers made of mullite, brown alumina and ceria foams under concentrated solar radiation. *Sol. Energy Mater Sol. Cells* **2019**, *194*, 121–129. [CrossRef]
23. Hoffschmidt, B.; Tellez, F.M.; Valverde, A.; Fernandez, J.; Fernandez, V. Performance evaluation of the 200-kWth HiTRec-II open volumetric air receiver. *J. Sol. Energy Eng.* **2003**, *125*, 87–94. [CrossRef]
24. Fend, T.; Pitz-Paal, R.; Reutter, O.; Bauerb, J.; Hoffschmidt, B. Two novel high-porosity materials as volumetric receivers for concentrated solar radiation. *Sol. Energy Mater. Sol. Cells* **2004**, *84*, 291–304. [CrossRef]
25. Behar, O.; Khellaf, A.; Mohammedi, K. A review of studies on central receiver solar thermal power plants. *Renew. Sustain. Energy Rev.* **2013**, *23*, 12–39. [CrossRef]
26. Ávila-Marín, A.L.; Alvarez-Lara, M.; Fernandez-Reche, J. Experimental results of gradual porosity wire mesh absorber for volumetric receivers. *Energy Procedia* **2014**, *49*, 275–283. [CrossRef]
27. Narushima, T.; Goto, T.; Hirai, T.; Iguchi, Y. High-temperature oxidation of silicon carbide and silicon nitride. *Mater. Trans.* **1997**, *38*, 821–835. [CrossRef]
28. Ding, S.; Zhu, S.; Zeng, Y.; Jiang, D. Fabrication of mullite-bonded porous silicon carbide ceramics by in situ reaction bonding. *J. Eur. Ceram. Soc.* **2007**, *27*, 2095–2102. [CrossRef]
29. Costa Oliveira, F.A.; Baxter, D.J. The effect of thermal cycling conditions on oxide scale structure and morphology on a hot-pressed silicon nitride. *J. Eur. Ceram. Soc.* **1999**, *19*, 2747–2756. [CrossRef]
30. Seuba, J.; Deville, S.; Guizard, C.; Stevenson, A.J. Mechanical properties and failure behavior of unidirectional porous ceramics. *Sci. Rep.* **2016**, *6*, 24326. [CrossRef]
31. Gibson, L.G.; Ashby, M.F. *Cellular Solids Structure & Properties*, 2nd ed.; Cambridge University Press: Cambridge, UK, 1997.
32. Baitalik, S.; Kayal, N. Thermal shock and chemical corrosion resistance of oxide bonded porous SiC ceramics prepared by infiltration technique. *J. Alloys Compd.* **2019**, *781*, 289–301. [CrossRef]
33. Brezny, R.; Green, D.J. Uniaxial strength behavior of brittle cellular materials. *J. Am. Ceram. Soc.* **1993**, *76*, 2185–2192. [CrossRef]
34. Orenstein, R.M.; Green, D.J. Thermal shock behavior of open-cell ceramic foams. *J. Am. Ceram. Soc.* **1992**, *75*, 1899–1905. [CrossRef]
35. Vedula, V.R.; Green, D.J.; Hellman, J.R. Thermal shock resistance of ceramic foams. *J. Am. Ceram. Soc.* **1999**, *82*, 649–656. [CrossRef]
36. Zaversky, F.; Sánchez, M.; Roldán, M.I.; Ávila-Marín, A.L.; Füssel, A.; Adler, J.; Knoch, M.; Dreitz, A. Experimental evaluation of volumetric solar absorbers—Ceramic foam vs. an innovative rotary disc absorber concept. *AIP Conf. Proc.* **2018**, *2033*, 040044.
37. Rodríguez, J.; Galindo, J.; Cañadas, I.; Monterreal, R.; Fernández-Reche, J. Desing and characterization of the new FAHEX100 concentrator of PSA's SF60 Solar Furnace. In Proceedings of the SolarPACES 2022, 28th International Conference on Concentrating Solar Power and Chemical Energy Systems, Albuquerque, NM, USA, 27–30 September 2022; Volume 1. [CrossRef]
38. *ASTM C1525-04*; Standard Test Method for Determination of Thermal Shock Resistance for Advanced Ceramics by Water Quenching. ASTM International: West Conshohocken, PA, USA, 2004.
39. Costa Oliveira, F.A.; Sardinha, M.; Galindo, J.; Rodríguez, J.; Cañadas, I.; Leite, M.; Fernandes, J.C. Manufacturing and thermal shock resistance of 3D-printed porous black zirconia for concentrated solar applications. *Crystals* **2023**, *13*, 1323. [CrossRef]